

Die Grenzen der
Chemie neu ausloten?
It takes
#HumanChemistry

Wir suchen kreative Chemikerinnen und Chemiker,
die mit uns gemeinsam neue Wege gehen wollen –
mit Fachwissen, Unternehmertum und Kreativität für
innovative Lösungen. Informieren Sie sich unter:

evonik.de/karriere

Sn-Pb Mixed Perovskites with Fullerene-Derivative Interlayers for Efficient Four-Terminal All-Perovskite Tandem Solar Cells

Hang Hu, Somayeh Moghadamzadeh, Raheleh Azmi, Yang Li, Milian Kaiser, Jan C. Fischer, Qihao Jin, Julia Maibach, Ihtez M. Hossain, Ulrich W. Paetzold,* and Bahram Abdollahi Nejangd*

Interfacial engineering is the key to high-performance perovskite solar cells (PSCs). While a wide range of fullerene interlayers are investigated for Pb-based counterparts with a bandgap of >1.5 eV, the role of fullerene interlayers is barely investigated in Sn-Pb mixed narrow-bandgap (NBG) PSCs. In this work, two novel solution-processed fullerene derivatives are investigated, namely indene-C60-propionic acid butyl ester and indene-C60-propionic acid hexyl ester (IPH), as the interlayers in NBG PSCs. It is found that the devices with IPH-interlayer show the highest performance with a remarkable short-circuit current density of 30.7 mA cm^{-2} and a low deficit in open-circuit voltage. The reduction in voltage deficit down to 0.43 V is attributed to reduced non-radiative recombination that the authors attribute to two aspects: 1) a higher conduction band offset of $\approx 0.2 \text{ eV}$ ($>0 \text{ eV}$) that hampers charge-carrier-back-transfer recombination; 2) a decrease in trap density at the perovskite/interlayer/ C_{60} interfaces that results in reduced trap-assisted recombination. In addition, incorporating the IPH interlayer enhances charge extraction within the devices that results in considerable enhancement in short-circuit current density. Using a NBG device with an IPH interlayer, a respectable power conversion efficiency of 24.8% is demonstrated in a four-terminal all-perovskite tandem solar cell.

Sn-Pb mixed narrow-bandgap (NBG) perovskites ($1.2\text{--}1.3 \text{ eV}$) bottom solar cells can overcome the detailed-balanced limit of single-junction devices.^[1–3] This technology promises to combine the ease of high efficiencies with low-temperature fabrication and solution processing.^[3,4] Despite the impressive power conversion efficiencies (PCEs) exceeding 25% for both all-perovskite four-terminal (4T) and two-terminal tandem solar cells,^[4,5] the low performance and stability of NBG perovskite sub-cells (with current record PCEs of $\approx 21.7\%$ ^[3–7]) still possesses a major hurdle in the exploitation of this all-thin-film tandem technology.^[1,4]

The key challenges of high-performance NBG perovskite solar cells (PSCs) are the low intrinsic material and device stability.^[4,8] The instabilities of Sn-based perovskites stem from fast oxidation of Sn^{2+} to Sn^{4+} even at very low oxygen content, leading to Sn vacancies inducing bulk and/or interfacial non-radiative recombination losses.^[9] Several attempts have

been proposed in literatures to suppress Sn oxidation, such as incorporating different antioxidant additives (e.g., SnF_2 ,^[10,11] SnCl_2 ,^[12] ascorbic acid,^[13] guanidinium thiocyanate,^[4] methylammonium thiocyanate,^[14] hydroxybenzene sulfonic acid,^[15]

1. Introduction

All-perovskite tandem solar cells combining Pb-based wide-bandgap (WBG) perovskites ($1.7\text{--}1.8 \text{ eV}$) top solar cells with

H. Hu, S. Moghadamzadeh, Y. Li, M. Kaiser, J. C. Fischer, I. M. Hossain, U. W. Paetzold, B. Abdollahi Nejang
Institute of Microstructure Technology (IMT)
Karlsruhe Institute of Technology (KIT)
Hermann-von-Helmholtz-Platz 1
76344 Eggenstein-Leopoldshafen, Germany
E-mail: ulrich.paetzold@kit.edu; bahram.abdollahi@kit.edu

 The ORCID identification number(s) for the author(s) of this article can be found under <https://doi.org/10.1002/adfm.202107650>.

© 2021 The Authors. Advanced Functional Materials published by Wiley-VCH GmbH. This is an open access article under the terms of the Creative Commons Attribution License, which permits use, distribution and reproduction in any medium, provided the original work is properly cited.

DOI: 10.1002/adfm.202107650

H. Hu, S. Moghadamzadeh, Y. Li, Q. Jin, I. M. Hossain, U. W. Paetzold, B. Abdollahi Nejang
Light Technology Institute (LTI)
Karlsruhe Institute of Technology (KIT)
Engesserstrasse 13, 76131 Karlsruhe, Germany
R. Azmi, J. Maibach
Institute for Applied Materials (IAM)
Karlsruhe Institute of Technology (KIT)
Hermann-von-Helmholtz-Platz 1
76344 Eggenstein-Leopoldshafen, Germany

tea polyphenol,^[16] and metallic Sn^[3,17,18]). It was also proven difficult to obtain uniform, pinhole-free, and high-quality Sn-based perovskite thin films due to the fast crystallization and film formation of solution-processed films.^[19] This rapid film formation may introduce defects on the surface and/or at the grain boundaries of the Sn-based perovskite thin films that initiate severe bulk and/or interfacial non-radiative recombination losses.^[19] To address the latter, several strategies were introduced to improve the film morphology of NBG perovskite thin films, including halide incorporation,^[20,21] two-step method,^[5,22] hot-casting method,^[23] gas quench processing,^[24] and vacuum-assisted growth control method.^[25]

Interfacial non-radiative recombination losses in PSCs correlate to not only the surface trap density, but the omitted presence of both charge carrier types at the interface, for example, by improper energy-level alignment or by charge-carrier back transfer.^[26,27] A perfect interface has minimal surface defects and favorable energy-level alignment.^[26] Interface-engineering strategies are widely used in perovskite photovoltaics to reduce interfacial non-radiative recombination that arises from point defects at the perovskite surface^[28,29] by reducing surface traps at the perovskite/transport layer (HTL) and/or perovskite/electron transport layer (ETL) interfaces.^[30–32] Previous studies have demonstrated that interfacial passivation at the NBG perovskite/HTL interface efficiently reduces the trap-assisted non-radiative recombination.^[33,34] Incorporating layered perovskites (2D) at the NBG perovskite/ETL interface to form 2D/3D hybrid structures improves the device efficiency and stability simultaneously.^[35–37] Unlike the pure Pb-based perovskites, tailoring effective passivating strategies (e.g., 2D/3D hybrid, graded junctions, or doping) to Sn-Pb based perovskites is still challenging due to a possible incorporation of excess of bulky organic cation,^[35] mismatch of surface energetics, and multiple defects, respectively.^[26]

Introduction of fullerene derivatives like conventional phenyl-C61-butyric acid methyl ester (PCBM) as an interlayer at the perovskite/ETL interface in Pb-based PSCs is an established strategy to reduce energy barrier and interfacial traps at this interface.^[32,38] Moreover, it serves as an efficient ETL for Pb-based PSCs due to its decent electron mobility and reduced resistance at the perovskite surface.^[38] Some fullerene derivatives were also successfully implemented in Sn-Pb mixed NBG PSCs to improve their performance. PCBM-interlayers introduced at Sn-Pb mixed perovskite/fullerene (C₆₀) interface, for example, were proven to significantly enhance open-circuit voltage (V_{OC}) in Sn-Pb mixed PSCs owing to reduced interfacial traps and thus resulting in less non-radiative recombination.^[39] Recently, A. Rajagopal and coauthors reported that the fullerene derivative graded fluoroalkyl-substituted fullerene (DF-C₆₀) is also suitable for an interlayer in NBG (CH₃NH₃Pb_{0.5}Sn_{0.5}I₃) PSCs.^[40] Their work demonstrated that the reduced trap sites at the surface of perovskite thin film lead to an improvement in device performance with a remarkably high V_{OC} of 0.89 V. These successful reports (see Table S1, Supporting Information) encourage exploring further fullerene-derivative interlayers and understanding their role/working principle for the performance and stability of NBG PSCs.

In this work, we report on previously unexplored fullerene derivatives as the interlayers in NBG PSCs. We systematically

study their effects on the performance and non-radiative recombination in the devices. We incorporate three fullerene-derivative interlayers: indene-C60-propionic acid butyl ester (IPB), indene-C60-propionic acid hexyl ester (IPH), and conventional PCBM into the perovskite/ETL interface. We identify IPH as the most effective interlayer in NBG PSCs, which delivers a higher conduction band offset (CBO) and accordingly suppresses the charge-carrier-back-transfer non-radiative recombination. Moreover, less trap-assisted non-radiative recombination is apparent in the devices with IPH-interlayer due to the reduced trap density at the perovskite/ETL interface. Both effects minimize non-radiative recombination and thereby reduce the V_{OC} deficit in the NBG PSCs with IPH-interlayer. In addition, incorporating IPH interlayer at the perovskite/ETL interface facilitates charge extraction that enables considerable enhancement in J_{SC}. As a result, the devices using IPH interlayer reach champion PCE of 18.6% with improved V_{OC} of 0.83 V and short-circuit current density (J_{SC}) of 30.7 mA cm⁻², which is superior to the devices with PCBM and without (w/o) an interlayer. Finally, we demonstrate 4T all-perovskite tandem solar cells with promising PCE of 24.8% (stabilized PCE of 23.7%), combining a semitransparent WBG (E_g = 1.63 eV) PSC and the best performing NBG (E_g = 1.26 eV) PSC developed in this work.

2. Results and Discussion

We utilize our previously presented strategy of vacuum-assisted growth control^[25,41] to fabricate pinhole-free and high-quality triple-cation NBG perovskite thin films. The perovskite has a composition of Cs_{0.025}(FA_{0.8}MA_{0.2})_{0.975}Sn_{0.5}Pb_{0.5}I₃ (referred to as CsFAMAPbSnI, E_g = 1.26 eV, Cs: cesium; FA: formamidinium; MA: methylammonium). The concentration of 2.5% Cs optimized in our previous work^[41] improves operational photo-stability for the NBG PSCs. We processed p-i-n planar PSCs in the layer sequence glass/indium tin oxide (ITO)/poly[bis(4-phenyl)(2,4,6-trimethylphenyl)amine] (PTAA)/CsFAMAPbSnI/interlayers/C₆₀/2,9-dimethyl-4,7-diphenyl-1,10-phenanthroline (BCP)/silver (Ag) (**Figure 1a**), with PCBM, IPB, or IPH fullerene-derivative interlayers (see Figure S1, Supporting Information for their chemical structures). The thickness of the perovskite thin films and interlayers are ≈600 and ≈8 nm, respectively (Figure S2, Supporting Information). Figure 1b shows that all NBG PSCs with interlayers investigated here improve the photovoltaic performance (see Figure S3a,b, Supporting Information). Our results reveal that each solar cell parameter (V_{OC}, FF, and J_{SC}) enhances and eventually each average PCE increases by 0.9%, 1.2%, and 1.8% for the PSCs with PCBM, IPB, and IPH-interlayers, respectively (Figure 1b). The IPH-interlayer yields the best-performing NBG PSC (PCE: 18.6%, V_{OC}: 0.83 V, J_{SC}: 30.7 mA cm⁻²) with stabilized PCE (SPCE) up to 18.0% as determined for maximum power point (MPP) tracking under continuous AM 1.5 G (1000 W m⁻²) irradiation for 5 min (Figure 1d). Noteworthy, the V_{OC} deficit (V_{OC, deficit} = E_g/q - V_{OC}) is merely 0.43 V for the best-performing NBG PSC with IPH-interlayer, which is among the lowest reported values for the Sn-Pb mixed PSCs (see Table S1, Supporting Information).^[7–9] However, IPH interlayer does not help to eliminate the hysteresis effect (see Figure S3c,d, Supporting Information). Considering that the

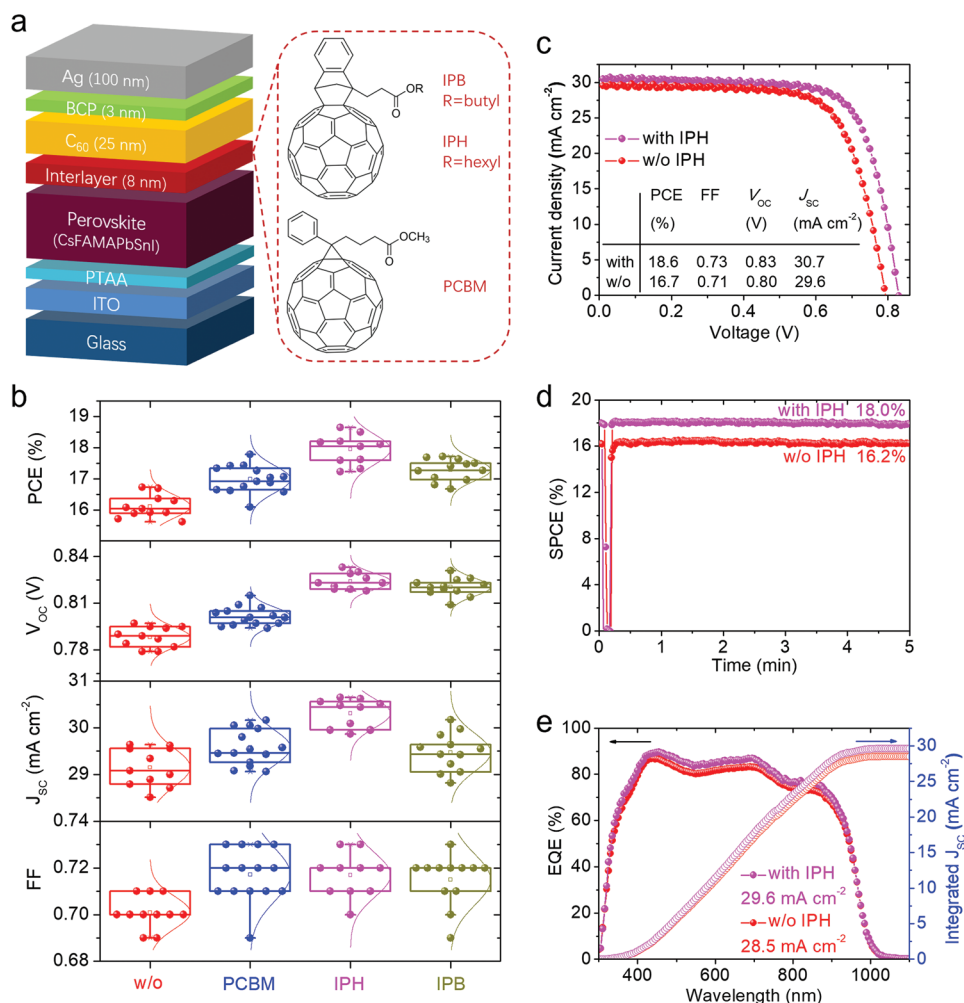


Figure 1. a) Schematic illustration of planar heterojunction PSCs based on NBG $\text{Cs}_{0.025}(\text{FA}_{0.8}\text{MA}_{0.2})_{0.975}\text{Sn}_{0.5}\text{Pb}_{0.5}\text{I}_3$ perovskite treated by different fullerene-derivative interlayers (PCBM, IPB, and IPH) and the corresponding molecule structures. b) Statistics of photovoltaic parameters distribution for NBG PSCs with different interlayers. c) Current-density–voltage (J – V) characteristics of champion devices with and without (w/o) IPH-interlayer measured from backward scan under AM 1.5 G (1000 W m^{-2}) irradiation. The inset shows the corresponding photovoltaic parameters. d) Stabilized power conversion efficiency (SPCE) under continuous illumination and e) external quantum efficiency (EQE) spectra of the corresponding best-performing devices. The shutter in front of the lamp was closed and only opened after 10 s when conducting the maximum power point (MPP) tracking in the beginning of 10 s. The J_{SC} values in (e) are the short-circuit current density values integrated from the EQE spectra.

enhanced J_{SC} for the NBG PSCs with IPH-interlayer results from a broadband enhancement in the external quantum efficiency (EQE) of these devices (Figure 1e), we study the optical spectra of the NBG perovskite thin films with and w/o an interlayer. As shown in Figure S4, Supporting Information, there are no significant changes in the optical properties after depositing different interlayers. Therefore, it can be rationalized that the fullerene-derivative interlayers at foremost improve the charge carrier extraction and not the light harvesting,^[38,39] as it will be investigated later in this work.

Proper energy-level alignment along with low trap density is key to obtain efficient extraction and low non-radiative recombination at the perovskite/ETL or perovskite/HTL interface.^[26,27] To start the discussion, it is important to know the energy levels of NBG perovskite and ETL. Ultraviolet photoelectron spectroscopy (UPS) assists us to explore the energy-level alignment of the NBG perovskite thin film and the investigated

fullerene-derivative interlayers (Figure 2). The highest occupied molecular orbital (HOMO) is extracted at the HOMO onset position (Figure 2a; Figure S5a, Supporting Information; right panel), while the work function is determined by the secondary electron cutoff (Figure 2a; Figure S5a, Supporting Information; left panel). The band gaps of these fullerene derivatives are estimated by Tauc-plots (see Figure S5b–h, Supporting Information). The lowest unoccupied molecular orbital (LUMO) is higher for PCBM, IPB, and IPH compared to C_{60} (Figure 2b). The highest LUMO of IPH or IPB enables high-lying electron quasi-Fermi level ($E_{f,e}$) in the perovskite-based p-i-n heterojunction under illumination. In contrary, the hole quasi-Fermi level ($E_{f,h}$), which is controlled by the energy alignment at the PTAA/perovskite interface, is similar for all the devices. Consequently, a higher quasi-Fermi level splitting between $E_{f,e}$ and $E_{f,h}$ encourages obtaining a higher V_{OC} for the devices with IPH and IPB interlayers.^[38,42] It is important to note that the

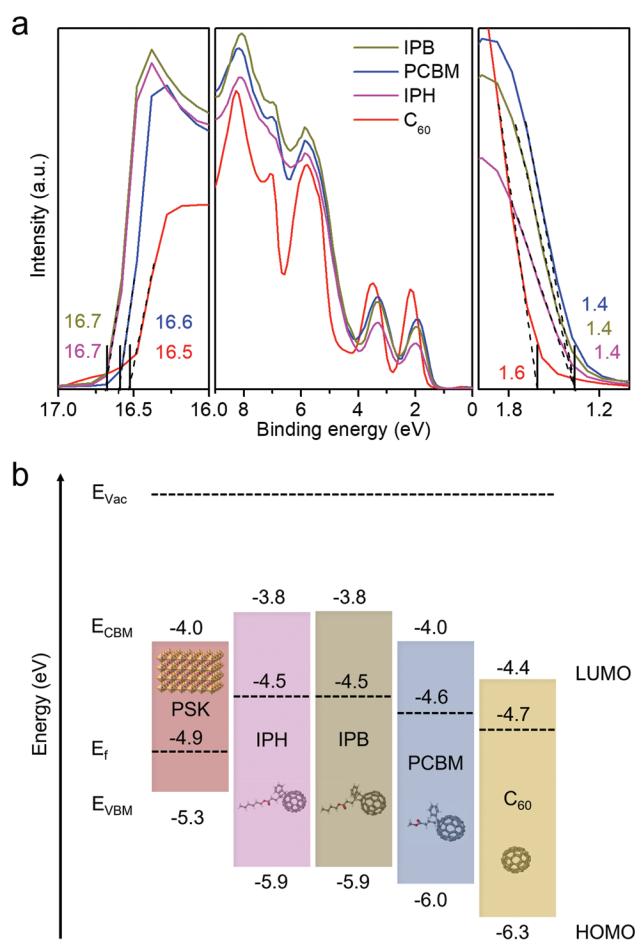


Figure 2. a) Ultra-violet photoelectron spectroscopy (UPS) spectra at the secondary electron cutoff, the valence region, and the HOMO onset position of different fullerene derivatives. b) Energy-level diagram for NBG perovskite and different fullerene derivatives with respect to the E_{vac} . E_{vac} : vacuum level; E_f : Fermi level; CBM: conduction band minimum; VBM: valence band maximum; HOMO: highest occupied molecular orbital; LUMO: lowest unoccupied molecular orbital.

higher LUMO levels of IPH and IPB compared to the LUMO level of C₆₀ as well as the conduction band minimum (CBM) of the NBG perovskite (Figure 2b), that is, the electron affinity of IPH and IPB is larger than that of NBG perovskite (Figure S6, Supporting Information), suggests a spike-like energy structure ($E_{LUMO(IPH)} > E_{CBM(PSK)}$) at perovskite/interlayer interface. This is in contrast to the cliff-like CBO with $E_{LUMO(C60)} < E_{CBM(PSK)}$ as apparent for the perovskite/C₆₀ interface, that is, higher CBM of the perovskite compared to the LUMO of C₆₀ with $CBO_{PSK/C60} = E_{LUMO(C60)} - E_{CBM(PSK)} < 0$ eV (see Figure S6, Supporting Information). In line with literature,^[39,43–46] we expect that a negative CBO does not impede the backward flow of photo-generated electrons from ETL to perovskite, and therefore triggers undesirable recombination of the photogenerated charge carriers at this interface leading to a reduction in V_{OC} of the device. On the contrary, when a spike-like CBO (>0 eV) is formed, it acts as a barrier and therefore the undesirable recombination at this interface is suppressed, which consequently results in enhanced V_{OC} . When the absolute value of CBO

increases, the activation energy ($E_a = E_g - |CBO|$) for charge carrier recombination decreases, resulting in increasing the probability of recombination at the perovskite/ETL interface.^[44,45] Therefore, an appropriate CBO is important to the interlayer and optimization of the perovskite/ETL interface. The possible recombination mechanism will be discussed later.

Having demonstrated that the IPH interlayer enhances the V_{OC} and J_{SC} of NBG PSCs, we study the effects of the interlayers on the device performance and non-radiative recombination utilizing material characterization and photophysical characterizations. Considering that non-radiative recombination centers often arise from surface or grain boundaries,^[19] we first probe the surface characteristics and Sn states toward the perovskite thin films. All perovskite thin films with and w/o different fullerene-derivative interlayers show similar morphology (Figure S7, Supporting Information) and bandgap (E_g at 1.26 eV, Figure S4d, Supporting Information). However, we observe lower roughness (Figure S7, Supporting Information) and larger contact angle (Figure S8, Supporting Information) for the perovskite thin films with different interlayers as the perovskite surficial groves are filled by fullerene derivatives. As discussed earlier, Sn cation vacancies are identified as non-radiative recombination centers in literature,^[47–51] but in this study, no detectable Sn 3d peak shifts are observed in X-ray photoelectron spectroscopy (XPS) for the perovskite thin films with different interlayers compared to the pristine perovskite thin films (Figure S9, Supporting Information). This suggests that the deposition of the fullerene derivatives on the NBG perovskite does not contribute as an oxidation barrier for Sn. Therefore, we conclude that introducing fullerene-derivative interlayers does not result in considerable differences in optical, morphological, and Sn-state properties. Furthermore, as fullerene-derivative covers both lateral grain-boundaries and grain surface in the interface of perovskite/C₆₀, in this work we define the interface a combination of grain-boundaries and grain surface.

To understand the origin of the V_{OC} improvement in the NBG PSCs with fullerene-derivative interlayers, we conduct steady-state photoluminescence (PL) and time-resolved PL (TRPL) to study the charge carrier dynamics. As shown in Figure 3a and Figure S10, Supporting Information, all fullerene derivatives in combination with C₆₀ serve as efficient PL quenchers. The perovskite thin films with C₆₀ or interlayer/C₆₀ show a significant reduction in PL intensity due to combined effects of 1) electron transfer from the perovskite to C₆₀ and 2) the trap-assisted non-radiative recombination.^[33,34] Meanwhile, the perovskite/IPH/C₆₀ layer sequence shows higher PL intensity compared to the perovskite/C₆₀ layer stack (Figure 3a), indicating enhanced band-to-band radiative recombination of free holes and electrons. We observe the same trend for the TRPL results (Figure 3b). Slow TRPL decay of perovskite/IPH/C₆₀ thin film (Table S2, Supporting Information), compared to that of the perovskite/C₆₀, indicates less trap-assisted non-radiative recombination.^[33,34,52]

Further evidence for the V_{OC} improvement by reduced non-radiative recombination losses is found in the variation of dark saturation current density (J_0) (Figure 3c) and ideality factor (n_{id}) (Figure 3d). We observe the reduced values of J_0 and n_{id} for all NBG PSCs with fullerene-derivative interlayers, hinting at less non-radiative recombination. As shown in Figure 3c,d,

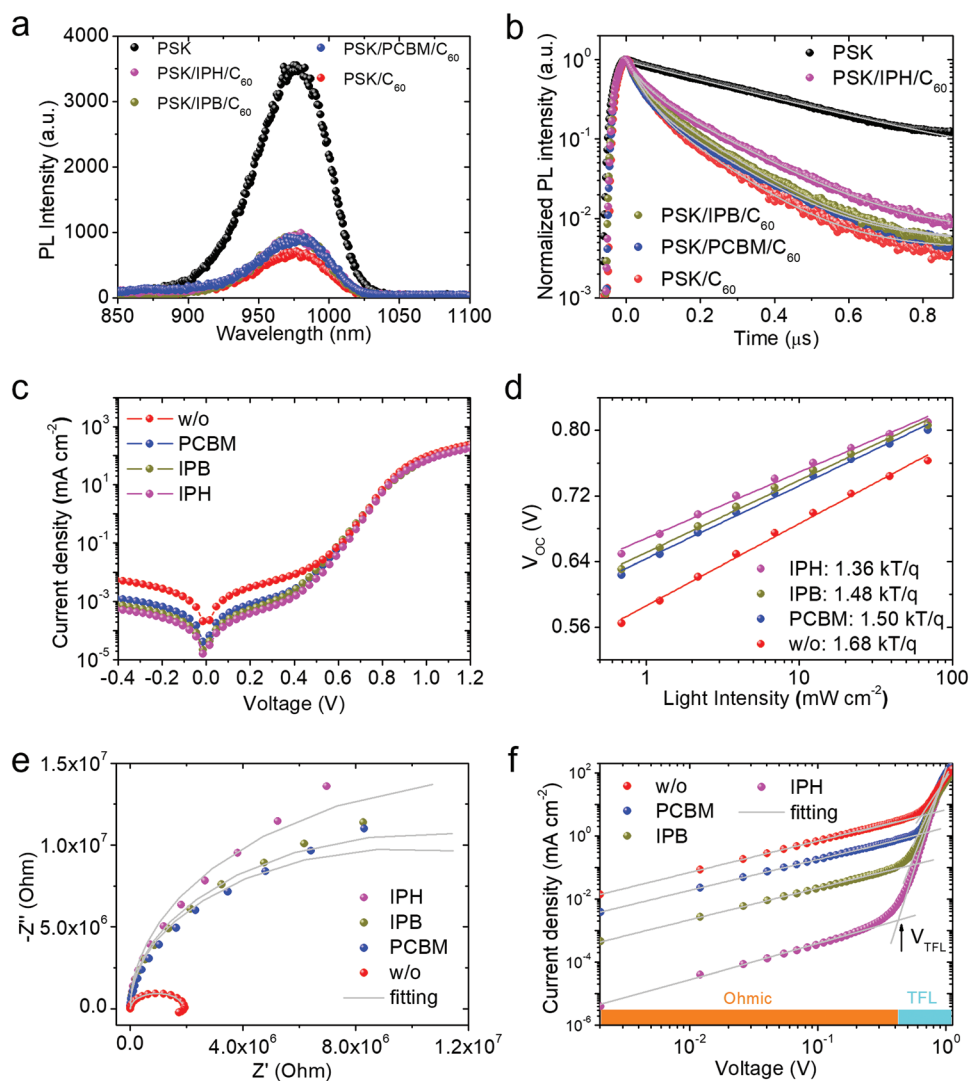


Figure 3. a) Steady-state photoluminescence (PL) and b) time-resolved photoluminescence (TRPL) of NBG perovskite thin film with and without (w/o) different fullerenes based on insulating AlO_x (via atomic layer deposition)/glass substrates. c) Dark current-density–voltage (J – V) characteristics, d) light intensity dependence of the V_{OC} , and e) Nyquist plots (symbols) and fitting curves (solid lines) of the best-performing PSCs with and without (w/o) an interlayer. f) Dark (J – V) characteristics of electron-only devices with and w/o an interlayer displaying V_{TFL} kink point behavior.

the NBG PSC with IPH-interlayer shows the lowest values of J_0 ($0.28 \times 10^{-7} \text{ mA cm}^{-2}$, see Figure S11, Supporting Information) and n_{id} (≈ 1.36) compared to those of the PSC w/o an interlayer ($J_0 = 1.23 \times 10^{-7} \text{ mA cm}^{-2}$, $n_{\text{id}} = 1.68$). The above-discussed data are in agreement and suggest that IPH-interlayer is efficient in reducing non-radiative recombination,^[21,53–56] leading to enhanced V_{OC} and accordingly PCE of the NBG PSCs.

To further verify the reduction of non-radiative recombination, we characterize the PSCs using electrical impedance spectroscopy (EIS), which benefits us to understand the dynamic process of charge-carrier recombination within devices. The impedance spectra at short-circuit condition are shown in Figure 3e, depicting considerable large semicircles in the low-frequency region of the Nyquist plots (whereas another very small semicircle in the high-frequency region is negligible, see Figure S12a, Supporting Information). This arc is related

to the charge recombination resistance (R_{rec}) at the perovskite/ETL interface,^[39,52,57] which is much higher than the charge transfer resistance (R_{ct}). Thus, the equivalent circuit is simplified to the (see Figure S12b, Supporting Information) composition of the series resistance (R_s) and the parallel resistance R_{rec} with recombination capacitance (C_{rec}). The larger semicircles (Figure 3e) reveal much higher R_{rec} values (Table S3, Supporting Information) for all devices with fullerene-derivative interlayers compared with the smaller R_{rec} for the device w/o an interlayer, which suggests a large recombination barrier within the devices with fullerene-derivative interlayers. In particular, we observe the highest and lowest values of R_{rec} for the PSC with IPH-interlayer (28.2 M Ω) and the PSC w/o an interlayer (1.9 M Ω), respectively. Simultaneously, the devices with interlayers show lower C_{rec} in the low-frequency region of capacitance–frequency (C – f) plots (Figure S12c, Supporting

Information) compared to the device w/o an interlayer. It indicates less ionic accumulation at the perovskite/IPH/C₆₀ interface by the introduction of IPH interlayer. The ionic accumulation could be linked to the trap-assisted non-radiative recombination.^[39] Thus, we estimate the charge carrier lifetime ($\tau_{\text{eis}} = R_{\text{rec}}C_{\text{rec}}$) of 203 ms for the device with IPH-interlayer, which is more than one order of magnitude higher than the lifetime of the device w/o an interlayer (14 ms). A longer τ_{eis} of the devices with IPH-interlayer indicates that photogenerated charge carriers have longer time for charge transfer (from perovskite layer to ETL) before possible recombination. The τ_{eis} values varied at different measuring condition (a light intensity or a bias) are very long here since we conducted EIS in the dark and with a bias of 0 V. Therefore, we believe τ_{eis} is a relative value and the value allows for quantitative analyses. The enhancement in τ_{eis} for the interlayer compared to the perovskite/C₆₀ reference is conclusive^[39,52] and in good agreement with reduced non-radiative recombination revealed by TRPL (see Figure 3b).

As discussed in the literatures, the interfacial trap states are closely associated with trap-assisted non-radiative recombination.^[26,27] Space-charge-limited-current (SCLC) is a technique to evaluate and estimate the trap density. We prepare so-called electron-only devices in the architecture ITO/CsFAMAPbSnI/IPH (with or w/o)/C₆₀/BCP/Ag for SCLC analyses. The dark current-density–voltage (J – V) characteristics of such devices with and w/o IPH-interlayer (Figure 3f; Figure S13, Supporting Information) is commonly differentiated in three regions: liner Ohmic region at low bias, trap-filled limited (TFL) region at intermediate bias, and nonlinear SCLC region at high bias. There is a kink point (see Figure 3f) between Ohmic and TFL regions that is defined as the trap-filling limit voltage (V_{TFL}), and thus the trap density (n_t) can be expressed from the following equation:^[3,58,59]

$$n_t = \frac{2V_{\text{TFL}}\epsilon\epsilon_0}{qL^2} \quad (1)$$

where L is the thickness of the perovskite thin film, ϵ is the relative dielectric constant of perovskite, ϵ_0 is the vacuum permittivity, and q is the elementary charge. We calculate the

trap density (an average value extracted from the same batch of the devices, see Figure S13e, Supporting Information) of $4.23 \times 10^{15} \text{ cm}^{-3}$ for the device with IPH-interlayer, which is much lower compared to that for the device w/o an interlayer ($6.26 \times 10^{15} \text{ cm}^{-3}$). This reduction in the trap density can be attributed to the suppression of interfacial trap states by the IPH-interlayer,^[28,38,40,49] which results in suppressed trap-assisted non-radiative recombination in the PSCs. These reduced traps may derive from the suppressed point defects in the grain-boundaries and grain surface of the perovskite thin films.^[28,29,60] Furthermore, we observe that the aged PSC with IPH-interlayer (stored in a nitrogen glove box for >1000 h) retains less non-radiative recombination, compared to the aged PSC w/o an interlayer (Figure S14a–c, Supporting Information). Consequently, the devices with IPH-interlayers (2.5 and 5 mg mL⁻¹) maintain $\approx 90\%$ of their initial PCE, whereas the device w/o an interlayer shows significant performance loss of $\approx 30\%$ after storage (Figure S14d, Supporting Information). Simultaneously, the aged devices with IPH-interlayers (5 mg mL⁻¹) exhibit better operational stability (Figure S14e, Supporting Information). The above results demonstrate that IPH-interlayer reduces the non-radiative recombination within NBG PSCs even in long-term inert storage.

In the following, we investigate the contribution of charge extraction to the J_{SC} enhancement in the devices with IPH-interlayer. The relationship between the photocurrent density (J_{ph}) and the effective voltage (V_{eff}) is often used to evaluate the charge extraction efficiency,^[61] or so-called exciton dissociation and charge carrier collection efficiency^[62,63] in organic solar cells. It is also used in PSCs to study the charge transport and charge collection properties for the interlayer in the Sn-based perovskite/HTL interface.^[34] Figure 4a illustrates normalized photocurrent density versus effective voltage ($J_{\text{ph}}/J_{\text{sat}} - V_{\text{eff}}$) characteristics for the devices with and w/o IPH-interlayer. J_{ph} is defined as $J_{\text{ph}} = J_{\text{L}} - J_{\text{D}}$, where J_{L} and J_{D} are the current densities under illumination and in dark, respectively.^[34,61,62] V_{eff} is determined as $V_{\text{eff}} = V_0 - V$, where V_0 is the voltage at which $J_{\text{ph}} = 0$ (V_0 is close to the built-in potential (V_{bi})^[62,63]) and V is the applied voltage. It is apparent that the J_{ph} increases linearly with the voltage for low V_{eff} values (<0.1 V), and at a

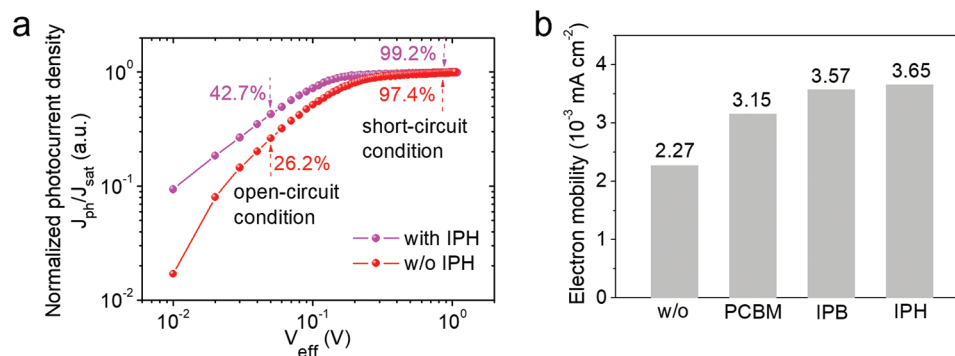


Figure 4. a) Normalized photocurrent density (J_{ph}) determined at AM 1.5 G (1000 W m⁻²) irradiation with the corresponding saturated value (J_{sat}) ($J_{\text{ph}}/J_{\text{sat}}$ presents charge extraction probability) as a function of the effective voltage (V_{eff}) for the NBG PSCs with and without (w/o) IPH-interlayer. The values of $J_{\text{ph}}/J_{\text{sat}}$ for devices with and w/o IPH-interlayer are 42.7% and 26.2% (both at open-circuit, $V_{\text{eff}} = 0.05$ V), 99.2% (at short-circuit, $V_{\text{eff}} = 0.88$ V), and 97.4% (at short-circuit, $V_{\text{eff}} = 0.85$ V), respectively. b) Comparison of electron mobility μ in electron-only devices with different interlayers. μ was determined by space-charge-limited-current (SCLC) method.

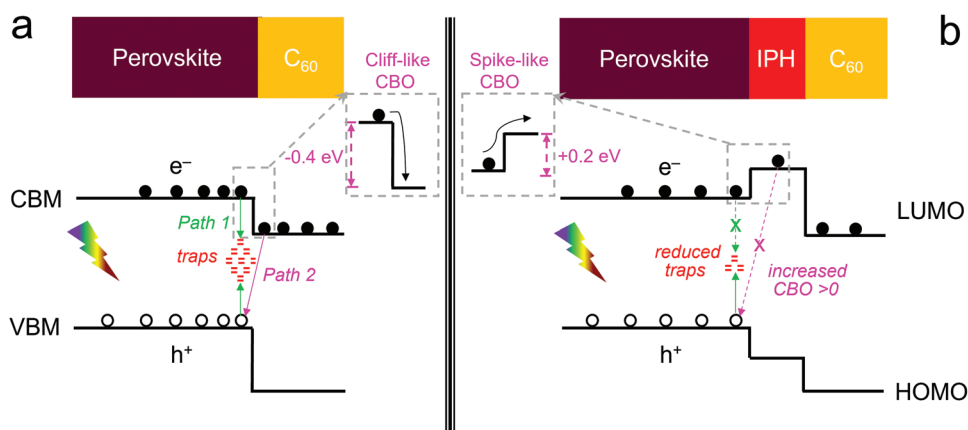


Figure 5. Schematic of the recombination process of charge carriers at the perovskite/ETL interface of a NBG PSC with a) a cliff-like and b) a spike-like conduction band offset. CBM: conduction band minimum; VBM: valence band maximum; HOMO: highest occupied molecular orbital; LUMO: lowest unoccupied molecular orbital; CBO: conduction band offset.

sufficiently high V_{eff} (>0.7 V) reaches its saturated value (J_{sat}) (see Figure S15a, Supporting Information). As expected, since the J_{sat} is only limited by the number of incident absorbed photons,^[55,56] the values of J_{sat} are similar for both devices with and w/o IPH-interlayer. This indicates that IPH interlayer does not contribute to EQE enhancement, which is in good agreement with the absorption results in Figure S4, Supporting Information. As a consequence, a higher J_{ph} is attributed to a higher charge extraction probability.^[34,61,62] The charge extraction probability ($J_{\text{ph}}/J_{\text{sat}}$) is calculated by normalizing J_{ph} to J_{sat} (see Figure 4a). We observe that the device with IPH-interlayer has a higher charge extraction probability across the full range from the open-circuit to short-circuit condition. The values of $J_{\text{ph}}/J_{\text{sat}}$ for the devices with and w/o IPH-interlayer are 42.7% and 26.2% (both at open-circuit, $V_{\text{eff}} = 0.05$ V), 99.2% (at short-circuit, $V_{\text{eff}} = 0.88$ V), and 97.4% (at short-circuit, $V_{\text{eff}} = 0.85$ V), respectively. These increased values of $J_{\text{ph}}/J_{\text{sat}}$ suggest that IPH interlayer enhances the charge extraction across the perovskite/ C_{60} interface, representing an increase in J_{SC} by ≈ 1 mA cm⁻² which is close to the enhancement in J_{SC} observed in our prototype devices ($\approx 2\%$ at the short-circuit condition). Further evidence of the relative reduction in charge carrier density (see Figure S15b, Experimental Section, Supporting Information) reveals less charge accumulation at the perovskite/IPH/ C_{60} interface.^[3,52,64,65] The improvement in charge extraction is expected to enhanced J_{SC} ^[34,61,62,66] and we suggest that it originates from an improved electron mobility^[34,38] within the devices (Figure 4b) and smaller electron capture radius^[67–69] for samples with IPH interlayer (see Figure S16, Experimental Section, Supporting Information).

Having studied the charge-carrier dynamics, we discuss possible pathways of non-radiative recombination within PSCs. Trap-assisted recombination and charge-carrier-back-transfer recombination are considered predominant pathways which contribute to the interfacial non-radiative recombination losses in PSCs.^[26] We propose the following mechanisms. 1) In the devices w/o an interlayer (see Figure 5a): the photogenerated charge carriers can recombine via the trap states (through path 1), which results in trap-assisted recombination; the backward flow of injected electrons (from C_{60} to perovskite layer)

would result in charge-carrier-back-transfer recombination due to the cliff-like CBO ($\text{CBO}_{\text{PSK}/\text{C}_{60}} = -0.4$ eV, see Figure S6, Supporting Information) effect (via path 2).^[39,43–46] 2) In the devices with IPH-interlayer (see Figure 5b): the reduced trap density (see Figure 3f) leads photogenerated charge carriers to escape from the trap states (through path 1), thus reducing trap-assisted recombination; a spike-like CBO ($\text{CBO}_{\text{PSK}/\text{IPH}} = 0.2$ eV, see Figure S6, Supporting Information) at the perovskite/IPH/ C_{60} interface provides a barrier to block the backward flow of injected electrons that hinders charge-carrier-back-transfer recombination (via path 2). In brief, summarizing all the experimental results, IPH stands out as the most efficient interlayer leading to high device performance with less non-radiative recombination. This improvement is mostly attributed to two aspects: 1) decreased trap density (n_{t}) minimizes trap-assisted recombination (via path) and 2) a higher CBO (>0 eV) provides large barrier of charge-carrier-back-transfer recombination (via path 2).

Last, we combine NBG PSCs ($E_{\text{g}} = 1.26$ eV) with IPH interlayer as the bottom solar cell with semitransparent WBG PSCs ($E_{\text{g}} = 1.63$ eV) as the top solar cell to configure 4T all-perovskite tandem solar cells. As reported in our previous work,^[41,70] the semitransparent top solar cell has a device configuration (Figure 6a) of glass/hydrogen-doped indium oxide $\text{In}_2\text{O}_3:\text{H}$ (IOH)/ SnO_2 nanoparticles/ $\text{Cs}_{0.1}(\text{FA}_{0.83}\text{MA}_{0.17})_{0.9}\text{Pb}(\text{I}_{0.83}\text{Br}_{0.17})_3/2,2',7,7'$ -tetrakis[*N,N*-di(4-methoxy-phenyl)amino]-9,9'-spirobifluorene (spiro-MeOTAD)/molybdenum oxide (MoO_x)/indium zinc oxide (IZO)/magnesium fluoride (MgF_2). A 165-nm IZO thin film, sputtered as the rear electrode onto 10-nm MoO_x thin film, protects the underlying spiro-MeOTAD layer and simultaneously acts as the hole blocking thin film.^[25,41,70,71] A 165-nm MgF_2 thin film serves as an antireflection coating to enhance the transmittance for improving light harvesting by NBG bottom solar cell.^[25,41,70,71] Figure 6b,c presents J - V characteristics and SPCE measurement of the best-performing single-junction WBG and NBG PSCs as well as the associated tandem solar cell, with the corresponding photovoltaic parameters summarized in Table 1. By applying a semitransparent filter (substrate area: 225 mm²; with the same structure and prepared under identical conditions as the semi-transparent WBG PSCs) atop, we obtain

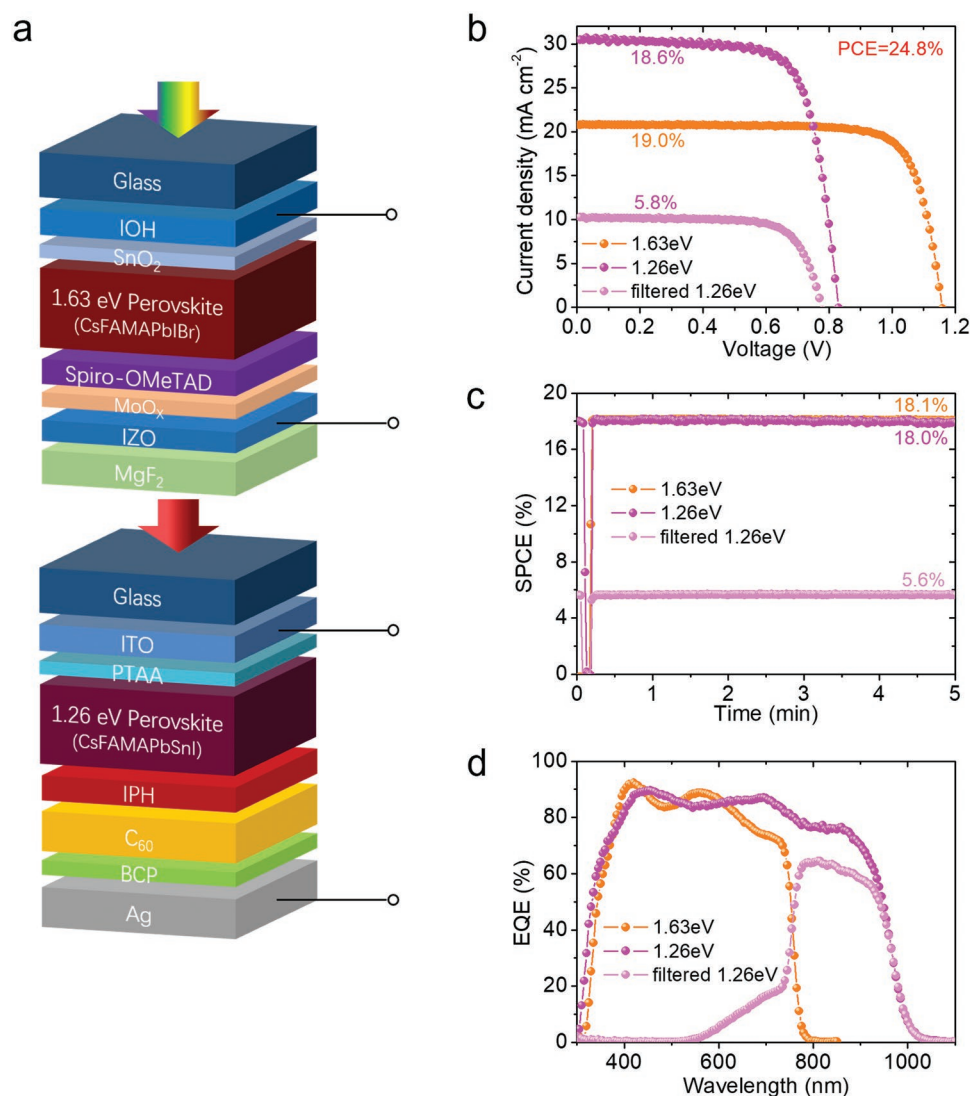


Figure 6. a) Schematic architecture of 4T all-perovskite tandem solar cells. b) J - V characteristics of the best-performing single-junction NBG bottom solar cell ($E_g = 1.26$ eV) with IPH-interlayer, WBG top solar cell ($E_g = 1.63$ eV), and filtered bottom solar cell measured from backward scan under AM 1.5 G (1000 W m^{-2}) irradiation. c) SPCE and d) EQE plots of the corresponding solar cells.

a PCE of 5.8% under backward scan and a SPCE of 5.6% for the best-performing NBG bottom solar cell with IPH-interlayer, which is higher than that of the device w/o an interlayer (PCE: 4.6%; SPCE: 4.3%, see Figure S16, Supporting Information). Adding PCE and SPCE values of the best-performing WBG top solar cell (19.0% and 18.1%, respectively) to that of the best-performing NBG bottom solar cell (filtered), we reach the best-performing 4T all-perovskite tandem solar cell with an outstanding PCE of 24.8% (=19.0% + 5.8%) and SPCE of 23.7% (=18.1% + 5.6%). The PCE improvement in tandem devices with IPH-interlayer mainly attributes to the enhancement of J_{SC} and V_{OC} in comparison with the device w/o an interlayer (Figure S17, Supporting Information). Moreover, the J_{SC} values integrated from EQE spectra (Figure 6d) for the top and bottom solar cells are 19.8 and 9.1 mA cm^{-2} , respectively, in good accordance with the values from J - V measurements. In brief, our work demonstrates that incorporation of IPH-interlayer

offers a promising route to manufacture highly efficient single-junction PSCs and the respective tandem solar cells.

3. Conclusion

In this work, we show that the novel fullerene derivative IPH serves as a promising interlayer in NBG PSCs attaining PCE of 18.6% (stabilized at 18.0%), accompanied by significant enhancement in V_{OC} and J_{SC} . Our observations based on UPS, PL, EIS, and SCLC analyses demonstrate that the enhanced V_{OC} upon implementing an IPH-interlayer is mostly attributed to minimized non-radiative recombination at the perovskite/ETL interface due to: 1) decreased trap density that results in decreased trap-assisted recombination; and 2) positive CBO (>0 eV) that suppresses charge-carrier-back-transfer recombination. Furthermore, the normalized photocurrent

Table 1. Summary of photovoltaic parameters for 4T tandem solar cells and the top and bottom solar cells measured in backward direction under AM 1.5 G (1000 W m⁻²).

	J_{SC} [mA cm ⁻²]	V_{OC} [V]	FF	PCE [%]	SPCE [%]
Top solar cell, 1.63 eV	20.8	1.16	0.79	19.0	18.1
Bottom solar cell, 1.26 eV (with IPH)	30.7	0.83	0.73	18.6	18.0
Bottom solar cell, 1.26 eV (with IPH, filtered)	10.1	0.78	0.74	5.8	5.6
4T tandem solar cell (with IPH)	–	–	–	24.8	23.7
Bottom solar cell, 1.26 eV (w/o IPH)	29.6	0.80	0.71	16.7	16.2
Bottom solar cell, 1.26 eV (w/o IPH, filtered)	9.0	0.74	0.69	4.6	4.3
4T tandem solar cell (w/o IPH)	–	–	–	23.6	22.4

J_{SC} : short-circuit current density; V_{OC} : open-circuit voltage; FF: fill factor; PCE: power conversion efficiency; SPCE: stabilized power conversion efficiency

density versus effective voltage and Mott–Schottky characterizations demonstrate that IPH-interlayer enhances the charge extraction at the interface that enables a higher J_{SC} . Finally, applying the best-performing NBG PCS with IPH-interlayer, we attain a 4T all-perovskite tandem solar cell with an outstanding PCE of 24.8% (stabilized at 23.7%).

Supporting Information

Supporting Information is available from the Wiley Online Library or from the author.

Acknowledgements

The authors would like to thank Moritz Schultes (KIT) and Erik Ahlswede (KIT) for providing the IOH substrates, and Karlsruhe Nano Micro Facility (KNMF) and Helmholtz Research Infrastructure at KIT for supporting UPS and XPS characterization. H.H. would like to acknowledge the Chinese Scholarship Council (CSC, no. 201808420221) for funding his doctoral research work. Financial support from the German Federal Ministry for Economic Affairs and Energy (CAPITANO, funding code: 03EE1038B), the Initiating and Networking funding of Helmholtz Association HYIG of U.W.P. (VH-NG-1148), the Helmholtz Energy Materials Foundry (HEMF), PEROSEED (ZT-0024), and Karlsruhe School of Optics and Photonics (KSOP) is gratefully acknowledged. B.A.N. acknowledges the financial support from the European Union's Horizon 2020 research and innovation program under the Marie Skłodowska-Curie (grant agreement no. 840937).

Open access funding enabled and organized by Projekt DEAL.

Conflict of Interest

The authors declare no conflict of interest.

Data Availability Statement

The data that support the findings of this study are available from the corresponding author upon reasonable request.

Keywords

all-perovskite tandem solar cells, charge extraction, fullerene derivatives, interlayers, non-radiative recombination, Sn-Pb mixed perovskites

Received: August 4, 2021
Revised: November 16, 2021
Published online:

- [1] G. E. Eperon, T. Leijtens, K. A. Bush, R. Prasanna, T. Green, J. T. W. Wang, D. P. McMeekin, G. Volonakis, R. L. Milot, R. May, A. Palmstrom, D. J. Slotcavage, R. A. Belisle, J. B. Patel, E. S. Parrott, R. J. Sutton, W. Ma, F. Moghadam, B. Conings, A. Babayigit, H. G. Boyen, S. Bent, F. Giustino, L. M. Herz, M. B. Johnston, M. D. McGehee, H. J. Snaith, *Science* **2016**, *354*, 861.
- [2] T. Leijtens, K. A. Bush, R. Prasanna, M. D. McGehee, *Nat. Energy* **2018**, *3*, 828.
- [3] R. Lin, K. Xiao, Z. Qin, Q. Han, C. Zhang, M. Wei, M. I. Saidaminov, Y. Gao, J. Xu, M. Xiao, A. Li, J. Zhu, E. H. Sargent, H. Tan, *Nat. Energy* **2019**, *4*, 864.
- [4] J. Tong, Z. Song, D. H. Kim, X. Chen, C. Chen, A. F. Palmstrom, P. F. Ndione, M. O. Reese, S. P. Dunfield, O. G. Reid, J. Liu, F. Zhang, S. P. Harvey, Z. Li, S. T. Christensen, G. Teeter, D. Zhao, M. M. Al-Jassim, M. F. A. M. Van Hest, M. C. Beard, S. E. Shaheen, J. J. Berry, Y. Yan, K. Zhu, *Science* **2019**, *364*, 475.
- [5] C. Li, Z. Song, C. Chen, C. Xiao, B. Subedi, S. P. Harvey, N. Shrestha, K. K. Subedi, L. Chen, D. Liu, Y. Li, Y. W. Kim, C.-s. Jiang, M. J. Heben, D. Zhao, R. J. Ellingson, N. J. Podraza, M. Al-Jassim, Y. Yan, *Nat. Energy* **2020**, *5*, 768.
- [6] D. Zhao, C. Chen, C. Wang, M. M. Junda, Z. Song, C. R. Grice, Y. Yu, C. Li, B. Subedi, N. J. Podraza, X. Zhao, G. Fang, R. G. Xiong, K. Zhu, Y. Yan, *Nat. Energy* **2018**, *3*, 1093.
- [7] G. Kapil, T. Bessho, T. Maekawa, A. K. Baranwal, Y. Zhang, M. A. Kamarudin, D. Hirotnani, Q. Shen, H. Segawa, S. Hayase, *Adv. Energy Mater.* **2021**, *11*, 2101069.
- [8] S. Gu, R. Lin, Q. Han, Y. Gao, H. Tan, J. Zhu, *Adv. Mater.* **2020**, *32*, 1907392.
- [9] C. Wang, Z. Song, C. Li, D. Zhao, Y. Yan, *Adv. Funct. Mater.* **2019**, *29*, 1808801.
- [10] L. Ma, F. Hao, C. C. Stoumpos, B. T. Phelan, M. R. Wasielewski, M. G. Kanatzidis, *J. Am. Chem. Soc.* **2016**, *138*, 14750.
- [11] S. Gupta, D. Cahen, G. Hodes, *J. Phys. Chem. C* **2018**, *122*, 13926.
- [12] C. M. Tsai, H. P. Wu, S. T. Chang, C. F. Huang, C. H. Wang, S. Narra, Y. W. Yang, C. L. Wang, C. H. Hung, E. W. G. Diau, *ACS Energy Lett.* **2016**, *1*, 1086.
- [13] X. Xu, C. C. Chueh, Z. Yang, A. Rajagopal, J. Xu, S. B. Jo, A. K. Y. Jen, *Nano Energy* **2017**, *34*, 392.
- [14] X. Lian, J. Chen, Y. Zhang, M. Qin, J. Li, S. Tian, W. Yang, X. Lu, G. Wu, H. Chen, *Adv. Funct. Mater.* **2019**, *29*, 1807024.
- [15] Q. Tai, X. Guo, G. Tang, P. You, T. W. Ng, D. Shen, J. Cao, C. K. Liu, N. Wang, Y. Zhu, C. S. Lee, F. Yan, *Angew. Chem., Int. Ed.* **2019**, *58*, 806.
- [16] H. Ban, Q. Sun, T. Zhang, H. Li, Y. Shen, M. Wang, *Sol. RRL* **2020**, *4*, 1900457.
- [17] Z. Zhu, N. Li, D. Zhao, L. Wang, A. K. Y. Jen, *Adv. Energy Mater.* **2019**, *9*, 1901826.
- [18] T. Jiang, Z. Chen, X. Chen, T. Liu, X. Chen, W. E. I. Sha, H. Zhu, Y. Yang, *Sol. RRL* **2020**, *4*, 1900467.
- [19] T. Yokoyama, D. H. Cao, C. C. Stoumpos, T. Bin Song, Y. Sato, S. Aramaki, M. G. Kanatzidis, *J. Phys. Chem. Lett.* **2016**, *7*, 776.
- [20] T. Leijtens, R. Prasanna, K. A. Bush, G. E. Eperon, J. A. Raiford, A. Gold-Parker, E. J. Wolf, S. A. Swifter, C. C. Boyd, H. P. Wang,

- M. F. Toney, S. F. Bent, M. D. McGehee, *Sustainable Energy Fuels* **2018**, *2*, 2450.
- [21] C. Li, Z. Song, D. Zhao, C. Xiao, B. Subedi, N. Shrestha, M. M. Junda, C. Wang, C. S. Jiang, M. Al-Jassim, R. J. Ellingson, N. J. Podraza, K. Zhu, Y. Yan, *Adv. Energy Mater.* **2019**, *9*, 1803135.
- [22] Y. Wang, W. Fu, J. Yan, J. Chen, W. Yang, H. Chen, *J. Mater. Chem. A* **2018**, *6*, 13090.
- [23] B. Zhao, M. Abdi-Jalebi, M. Tabachnyk, H. Glass, V. S. Kamboj, W. Nie, A. J. Pearson, Y. Puttison, K. C. Gödel, H. E. Beere, D. A. Ritchie, A. D. Mohite, S. E. Dutton, R. H. Friend, A. Sadhanala, *Adv. Mater.* **2017**, *29*, 1604744.
- [24] J. Werner, T. Moot, T. A. Gossett, I. E. Gould, A. F. Palmstrom, E. J. Wolf, C. C. Boyd, M. F. A. M. Van Hest, J. M. Luther, J. J. Berry, M. D. McGehee, *ACS Energy Lett.* **2020**, *5*, 1215.
- [25] B. Abdollahi Nejand, I. M. Hossain, M. Jakoby, S. Moghadamzadeh, T. Abzieher, S. Gharibzadeh, J. A. Schwenzer, P. Nazari, F. Schackmar, D. Hauschild, L. Weinhardt, U. Lemmer, B. S. Richards, I. A. Howard, U. W. Paetzold, *Adv. Energy Mater.* **2020**, *10*, 1902583.
- [26] D. Luo, R. Su, W. Zhang, Q. Gong, R. Zhu, *Nat. Rev. Mater.* **2020**, *5*, 44.
- [27] C. M. Wolff, P. Capioglio, M. Stolterfoht, D. Neher, *Adv. Mater.* **2019**, *31*, 1902762.
- [28] J. M. Ball, A. Petrozza, *Nat. Energy* **2016**, *1*, 16149.
- [29] J. Huang, Y. Yuan, Y. Shao, Y. Yan, *Nat. Rev. Mater.* **2017**, *2*, 17042.
- [30] S. D. Stranks, *ACS Energy Lett.* **2017**, *2*, 1515.
- [31] M. Stolterfoht, C. M. Wolff, J. A. Márquez, S. Zhang, C. J. Hages, D. Rothhardt, S. Albrecht, P. L. Burn, P. Meredith, T. Unold, D. Neher, *Nat. Energy* **2018**, *3*, 847.
- [32] S. Li, K. Fan, Y. Cui, S. Leng, Y. Ying, W. Zou, Z. Liu, C. Z. Li, K. Yao, H. Huang, *ACS Energy Lett.* **2020**, *5*, 2015.
- [33] S. Shao, Y. Cui, H. Duim, X. Qiu, J. Dong, G. H. ten Brink, G. Portale, R. C. Chiechi, S. Zhang, J. Hou, M. A. Loi, *Adv. Mater.* **2018**, *30*, 1803703.
- [34] G. Xu, P. Bi, S. Wang, R. Xue, J. Zhang, H. Chen, W. Chen, X. Hao, Y. Li, Y. Li, *Adv. Funct. Mater.* **2018**, *28*, 1804427.
- [35] M. Wei, K. Xiao, G. Walters, R. Lin, Y. Zhao, M. I. Saidaminov, P. Todorović, A. Johnston, Z. Huang, H. Chen, A. Li, J. Zhu, Z. Yang, Y. K. Wang, A. H. Proppe, S. O. Kelley, Y. Hou, O. Voznyy, H. Tan, E. H. Sargent, *Adv. Mater.* **2020**, *32*, 1907058.
- [36] C. Li, Y. Pan, J. Hu, S. Qiu, C. Zhang, Y. Yang, S. Chen, X. Liu, C. J. Brabec, M. K. Nazeeruddin, Y. Mai, F. Guo, *ACS Energy Lett.* **2020**, *5*, 1386.
- [37] W. Ke, C. Chen, I. Spanopoulos, L. Mao, I. Hadar, X. Li, J. M. Hoffman, Z. Song, Y. Yan, M. G. Kanatzidis, *J. Am. Chem. Soc.* **2020**, *142*, 15049.
- [38] P. W. Liang, C. C. Chueh, S. T. Williams, A. K. Y. Jen, *Adv. Energy Mater.* **2015**, *5*, 1402321.
- [39] G. Kapil, T. S. Ripolles, K. Hamada, Y. Ogomi, T. Bessho, T. Kinoshita, J. Chantana, K. Yoshino, Q. Shen, T. Toyoda, T. Minemoto, T. N. Murakami, H. Segawa, S. Hayase, *Nano Lett.* **2018**, *18*, 3600.
- [40] A. Rajagopal, P. W. Liang, C. C. Chueh, Z. Yang, A. K. Y. Jen, *ACS Energy Lett.* **2017**, *2*, 2531.
- [41] S. Moghadamzadeh, I. M. Hossain, T. Duong, S. Gharibzadeh, T. Abzieher, H. Pham, H. Hu, P. Fassel, U. Lemmer, B. Abdollahi Nejand, U. W. Paetzold, *J. Mater. Chem. A* **2020**, *8*, 24608.
- [42] A. Rajagopal, Z. Yang, S. B. Jo, I. L. Braly, P. W. Liang, H. W. Hillhouse, A. K. Y. Jen, *Adv. Mater.* **2017**, *29*, 1702140.
- [43] C. Ding, Y. Zhang, F. Liu, Y. Kitabatake, S. Hayase, T. Toyoda, K. Yoshino, T. Minemoto, K. Katayama, Q. Shen, *Nano Energy* **2018**, *53*, 17.
- [44] T. Minemoto, T. Matsui, H. Takakura, Y. Hamakawa, T. Negami, Y. Hashimoto, T. Uenoyama, M. Kitagawa, *Sol. Energy Mater. Sol. Cells* **2001**, *67*, 83.
- [45] T. Minemoto, M. Murata, *Sol. Energy Mater. Sol. Cells* **2015**, *133*, 8.
- [46] Y. Raoui, H. Ez-Zahraoui, S. Kazim, S. Ahmad, *J. Energy Chem.* **2021**, *54*, 822.
- [47] I. Chung, J. H. Song, J. Im, J. Androulakis, C. D. Malliakas, H. Li, A. J. Freeman, J. T. Kenney, M. G. Kanatzidis, *J. Am. Chem. Soc.* **2012**, *134*, 8579.
- [48] M. H. Kumar, S. Dharani, W. L. Leong, P. P. Boix, R. R. Prabhakar, T. Baikie, C. Shi, H. Ding, R. Ramesh, M. Asta, M. Graetzel, S. G. Mhaisalkar, N. Mathews, *Adv. Mater.* **2014**, *26*, 7122.
- [49] E. Aydin, M. De Bastiani, S. De Wolf, *Adv. Mater.* **2019**, *31*, 1900428.
- [50] P. Schulz, D. Cahen, A. Kahn, *Chem. Rev.* **2019**, *119*, 3349.
- [51] X. Zheng, Y. Hou, C. Bao, J. Yin, F. Yuan, Z. Huang, K. Song, J. Liu, J. Troughton, N. Gasparini, C. Zhou, Y. Lin, D. J. Xue, B. Chen, A. K. Johnston, N. Wei, M. N. Hedhili, M. Wei, A. Y. Alsalloum, P. Maity, B. Turedi, C. Yang, D. Baran, T. D. Anthopoulos, Y. Han, Z. H. Lu, O. F. Mohammed, F. Gao, E. H. Sargent, O. M. Bakr, *Nat. Energy* **2020**, *5*, 131.
- [52] T. Bu, J. Li, F. Zheng, W. Chen, X. Wen, Z. Ku, Y. Peng, J. Zhong, Y. B. Cheng, F. Huang, *Nat. Commun.* **2018**, *9*, 4609.
- [53] X. Zhu, D. Yang, R. Yang, B. Yang, Z. Yang, X. Ren, J. Zhang, J. Niu, J. Feng, S. Liu, *Nanoscale* **2017**, *9*, 12316.
- [54] F. Li, Y. Xie, Y. Hu, M. Long, Y. Zhang, J. Xu, M. Qin, X. Lu, M. Liu, *ACS Energy Lett.* **2020**, *5*, 1422.
- [55] M. Zhang, Q. Chen, R. Xue, Y. Zhan, C. Wang, J. Lai, J. Yang, H. Lin, J. Yao, Y. Li, L. Chen, Y. Li, *Nat. Commun.* **2019**, *10*, 4593.
- [56] W. Q. Wu, P. N. Rudd, Q. Wang, Z. Yang, J. Huang, *Adv. Mater.* **2020**, *32*, 2000995.
- [57] H. Hu, B. Dong, H. Hu, F. Chen, M. Kong, Q. Zhang, T. Luo, L. Zhao, Z. Guo, J. Li, Z. Xu, S. Wang, D. Eder, L. Wan, *ACS Appl. Mater. Interfaces* **2016**, *8*, 17999.
- [58] Q. Dong, Y. Fang, Y. Shao, P. Mulligan, J. Qiu, L. Cao, J. Huang, *Science* **2015**, *347*, 967.
- [59] D. Shi, V. Adinolfi, R. Comin, M. Yuan, E. Alarousu, A. Buin, Y. Chen, S. Hoogland, A. Rothenberger, K. Katsiev, Y. Losovyj, X. Zhang, P. A. Dowben, O. F. Mohammed, E. H. Sargent, O. M. Bakr, *Science* **2015**, *347*, 519.
- [60] M. J. Trimpl, A. D. Wright, K. Schutt, L. R. V. Buizza, Z. Wang, M. B. Johnston, H. J. Snaith, P. Müller-Buschbaum, L. M. Herz, *Adv. Funct. Mater.* **2020**, *30*, 2004312.
- [61] J. De Chen, C. Cui, Y. Q. Li, L. Zhou, Q. D. Ou, C. Li, Y. Li, J. X. Tang, *Adv. Mater.* **2015**, *27*, 1035.
- [62] A. K. Kyaw, D. H. Wang, D. Wynands, J. Zhang, T. Q. Nguyen, G. C. Bazan, A. J. Heeger, *Nano Lett.* **2013**, *13*, 3796.
- [63] Y. Xie, W. Zhou, J. Yin, X. Hu, L. Zhang, X. Meng, Q. Ai, Y. Chen, *J. Mater. Chem. A* **2016**, *4*, 6158.
- [64] Y. Wang, K. Wang, W. S. Subhani, C. Zhang, X. Jiang, S. Wang, H. Bao, L. Liu, L. Wan, S. Liu, *Small* **2020**, *16*, 1907283.
- [65] G. Yang, C. Wang, H. Lei, X. Zheng, P. Qin, L. Xiong, X. Zhao, Y. Yan, G. Fang, *J. Mater. Chem. A* **2017**, *5*, 1658.
- [66] J. Shi, Y. Li, Y. Li, D. Li, Y. Luo, H. Wu, Q. Meng, *Joule* **2018**, *2*, 879.
- [67] M. Kuik, L. J. A. Koster, G. A. H. Wetzelaer, P. W. M. Blom, *Phys. Rev. Lett.* **2011**, *107*, 256805.
- [68] S. Shao, M. Abdu-Aguye, L. Qiu, L. H. Lai, J. Liu, S. Adjokate, F. Jahani, M. E. Kamminga, G. H. Ten Brink, T. T. M. Palstra, B. J. Kooi, J. C. Hummelen, M. Antonietta Loi, *Energy Environ. Sci.* **2016**, *9*, 2444.
- [69] D. Yang, X. Zhang, K. Wang, C. Wu, R. Yang, Y. Hou, Y. Jiang, S. Liu, S. Priya, *Nano Lett.* **2019**, *19*, 3313.
- [70] S. Moghadamzadeh, I. M. Hossain, M. Loy, D. B. Ritzer, H. Hu, D. Hauschild, A. Mertens, J.-P. Becker, A. A. Haghighirad, E. Ahlswede, L. Weinhardt, U. Lemmer, B. Abdollahi Nejand, U. W. Paetzold, *ACS Appl. Mater. Interfaces* **2021**, *13*, 46488.
- [71] S. Gharibzadeh, I. M. Hossain, P. Fassel, B. Abdollahi Nejand, T. Abzieher, M. Schultes, E. Ahlswede, P. Jackson, M. Powalla, S. Schäfer, M. Rienäcker, T. Wietler, R. Peibst, U. Lemmer, B. S. Richards, U. W. Paetzold, *Adv. Funct. Mater.* **2020**, *30*, 1909919.